My latest paper to CED

by Foek Tjong Wong

Submission date: 29-Apr-2022 01:09PM (UTC+0700)
Submission ID: 1823588508
File name: m_Elements_using_an_Improved_Implementation_of_the_DGS_2022.pdf (536.27K)
Word count: 6066
Character count: 29505

Civil Engineering Dimension, Vol. 24, No. 1, March 2022, 11-18 DOI: 10.9744/CED.24.1.11-18
ISSN 1410-9530 print / ISSN 1979-570X online

Locking-free Kriging-based Timoshenko Beam Elements using an Improved Implementation of the Discrete Shear Gap Technique

Wong, F.T.[1*], Santoso, S.W.[2], and Sutrisno, M.[1]

Abstract: Kriging-based finite element method (K-FEM) is an enhancement of the conventional finite element method using a Kriging interpolation as the trial solution in place of a polynomial function. In the application of the K-FEM to the Timoshenko beam model, the discrete shear gap (DSG) technique has been employed to overcome the shear locking difficulty. However, the applied DSG was only effective for the Kriging-based beam element with a cubic basis and three element-layer domain of influencing nodes. Therefore, this research examines a modified implementation of the DSG by changing the substitute DSG field from the Kriging-based interpolation to linear interpolation of the shear gaps at the element nodes. The results show that the improved elements of any polynomial degree are free from shear locking. Furthermore, the results of beam deflection, cross-section rotation, and bending moment are very accurate, while the shear force field is piecewise constant.

Keywords: Kriging-based finite element method; Timoshenko beam; shear locking; discrete shear gap.

Introduction

Kriging-based finite element method (K-FEM) is an enhancement of the standard finite element method (FEM) using a Kriging interpolation (KI) as the trial solution in place of a polynomial interpolation [1-3]. In this method, KI is constructed for each element using a set of nodes including the element nodes and nodes of several layers of surrounding elements (called *satellite nodes*). This element and its surrounding elements constitute a domain of influencing nodes (DOI). Accordingly, the global trial solution is in the form of "element-by-element" piecewise Kriging interpolation. The key advantages of the K-FEM are first, remarkable accurate solutions of the field variables and their gradients can be achieved even though using the simplest elements, that is, three-node triangular elements in 2D problems and four-node tetrahedral elements in 3D problems. Secondly, solution refinement can be achieved without any change to the mesh. Lastly, K-FEM computational procedure is similar to the standard FEM so that an existing finite element computer program can be modified with ease to include the K-FEM.

[1] Department of Civil Engineering, Petra Christian University, Surabaya, INDONESIA
[2] Structural Engineer, Federal Engineering Consultant Inc., Taipei, TAIWAN
*Corresponding author; Email: wftjong@petra.ac.id

Note: Discussion is expected before July, 1st 2022, and will be published in the "Civil Engineering Dimension", volume 24, number 2, September 2022.

Received 22 January 2021; revised 22 November 2021; accepted 20 December 2021.

A drawback of the K-FEM is that in 2D and 3D problems, the global trial solution is discontinuous across element boundaries. In other words, the Kriging-based elements are nonconforming. The issue of non-conformity and its effects on the convergence characteristics has been addressed in Reference [4]. It was found that despite the non-conformity, solutions of the K-FEM with a quartic spline correlation function and appropriate Kriging parameters always converge to the exact solutions. The adverse effect is that the convergence rate and accuracy of the K-EFM with a higher degree polynomial basis may not be better than with a lower degree polynomial basis. Another drawback of the K-FEM is that its computational cost is higher than the standard FEM. This is primarily because the Kriging interpolation does not have an explicit expression; it is constructed for each element during the computer running process [1].

In the development of K-FEM for analyses of shear deformable beams, plates, and shells, as in the conventional FEM, the numerical difficulty of shear locking and membrane locking occurred [5-8]. In the K-FEM for the Timoshenko beam model [7], the longstanding selective-reduced integration technique (SRI) has been utilized to eliminate the shear locking. The results showed that the SRI is effective at eliminating the locking. However, the use of the SRI made the results for the case of thick beams less accurate and produced erroneous shear force distribution (except at the element center).

Subsequently, a more recent approach for eliminating shear locking, namely the discrete shear gap (DSG)

technique [9-10], was applied in the K-FEM for analysis of Timoshenko beams [8]. 'Shear gap' at a beam point x is defined as the increment of the deflection due to shear deformation from a reference point x_0. 'Discrete' shear gaps are shear gaps at the nodal points. In the standard FEM for the Timoshenko beam model [11], the DSGs were evaluated at the element nodal points. In the K-FEM [8], however, the DSGs were evaluated at all nodes in a DOI and interpolated using Kriging shape functions to create a substitute shear gap field. A substitute shear strain field, γ-bar, was then obtained by differentiating the substitute shear gap. The original displacement-based shear strain, γ, was replaced with the substitute shear strain to circumvent the shear locking. The numerical tests showed that Kriging-based Timoshenko elements with the DSG were free from shear locking only for a cubic polynomial basis with three element layers and a linear basis with one element layer, which is identical as the standard two-node Timoshenko beam element. The elements with other polynomial bases or other numbers of element layers suffered from shear locking.

This paper presents a modified implementation of the DSG technique to eliminate the shear locking in the application of Kriging-based Timoshenko beam elements with any degree of polynomial basis function. The DSGs are evaluated only at the element end nodes in this work, not at all nodes in the DOI as in the previous work [8]. The substitute shear gap field is then constructed using standard linear shape functions, not Kriging shape functions. Accordingly, the resulting substitute shear strain field is constant over an element. A series of numerical tests are carried out to study the effectiveness of eliminating shear locking, accuracy, and convergence. The results show that the Kriging-based Timoshenko beam elements using the present implementation of the DSG technique are indeed free from shear locking.

Kriging-based Finite Element Method for Timoshenko Beams

Weak Form of the Governing Equations

Consider a Timoshenko beam model with the global Cartesian coordinate system and positive sign conventions for the deflection, w, cross-section rotation, θ, internal bending moment, M, and shear force, Q, as shown in Figure 1. The geometrical and material parameters of the beam are the beam length, L, the cross-sectional area, A, the cross-sectional moment of inertia about the y axis, I, the modulus of elasticity E, and the shear modulus G. For example (see Fig 1(b)), the beam is subjected to a distributed load q, a concentrated load P_0, and a moment M_0 at the left end (at $x = 0$). At the right end, the beam is subjected to a prescribed deflection w_L and a prescribed rotation θ_L (see Fig 1(b)), $w_L = \theta_L = 0$ if the right end is clamped. The weak form of the governing equations for the beam static deformation is given as [12]

$$\int_0^L \delta\theta_{,x}\, EI\, \theta_{,x}\, dx + \int_0^L (\delta w_{,x} - \delta\theta) GA_s (w_{,x} - \theta) dx = \int_0^L \delta w q\, dx + \delta w(0) P_0 + \delta\theta(0) M_0 \;\forall\, \delta w, \delta\theta \in \mathbb{V} = \{v | v \in \mathbb{H}^1(0, L), v(L) = 0\} \quad (1)$$

In words, this integral equation states that if $w = w(x)$ and $\theta = \theta(x)$ are the exact solutions, then the equation should be true for any admissible weighting functions $\delta w = \delta w(x)$ and $\delta\theta = \delta\theta(x)$. The weak form equation implicitly contains the beam equilibrium equations and force boundary conditions (see the derivation in Reference [12]). The weak form is identical to the principle of virtual displacement where δw and $\delta\theta$ are the virtual deflection and virtual rotation, respectively. The comma denotes the derivative to the variable following it. Symbol A_s is the effective shear area of the cross-section, that is, $A_s = kA$, where k is a shear correction factor depending upon the cross-section geometry. The second line of the equation means that the integral equation is applicable for all δw and $\delta\theta$ in the space of admissible weighting functions, $\mathbb{V}$. Space $\mathbb{H}^1(0, L)$ is the Sobolev function space of first degree [13-14], that is,

$$\mathbb{H}^1(0, L) = \{v | \int_0^L (v^2 + L^2 v_{,x}^2) dx < \infty\} \quad (2)$$

The model problem is to find $w \in \mathbb{S}_w = \{w | w \in \mathrm{H}^1(0, L),\ w(L) = w_L\}$ and $\theta \in \mathbb{S}_\theta = \{\theta | \theta \in \mathrm{H}^1(0, L), \theta(L) = \theta_L\}$ such that eqn. (1) is satisfied for all $\delta w, \delta\theta \in \mathbb{V}$.

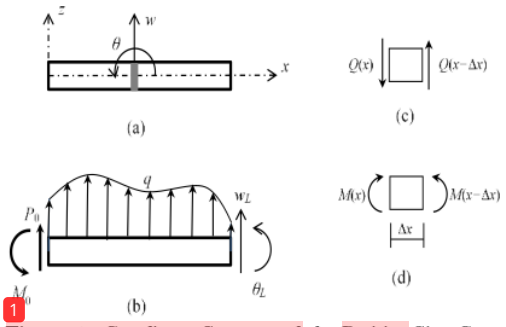

Figure 1. Coordinate System and the Positive Sign Convention for the Beam Deflection, w, Cross-section Rotation, θ(a); External Loads q, P_0, M_0, Support Conditions w_L, θ_L(b); Internal Shear Force(c), Q and Bending Moment, M(d)

Once the solution for w and θ has been obtained, the bending moment and shear stress distributions along the beam can be obtained using

$$M = EI_y w_{,xx} \quad (3)$$

$$Q = GA_s (w_{,x} - \theta) \quad (4)$$

Kriging-based Finite Element Formulation

For convenience in the subsequent finite element formulation, the displacement boundary conditions at the beam right end are temporarily removed. Let the beam be subdivided into N_e elements and N_p nodes and consider an element with its surrounding elements, which constitutes a two-layer element DOI covering n nodes as illustrated in Fig 2. The unknown field variables over the element are approximated as follows:

$$w \approx w^h = \mathbf{N}_w \mathbf{d} \tag{5a}$$

$$\theta \approx \theta^h = \mathbf{N}_\theta \mathbf{d} \tag{6a}$$

where

$$\mathbf{N}_w = [N_1(x) \quad 0 \quad N_2(x) \quad 0 \quad \cdots \quad N_n(x) \quad 0] \tag{5b}$$

$$\mathbf{N}_\theta = [0 \quad N_1(x) \quad 0 \quad N_2(x) \quad \cdots \quad 0 \quad N_n(x)] \tag{6b}$$

are the matrix of Kriging shape functions for the deflection and rotation, respectively, and

$$\mathbf{d} = [w_1 \quad \theta_1 \quad w_2 \quad \theta_2 \quad \cdots \quad w_n \quad \theta_n]^{\mathrm{T}} \tag{5c}$$

is the vector of nodal displacements. The indices here use a local numbering system in the DOI. The number of nodes in the DOI, n, depends on the number of elements used in the DOI and is different for the interior and exterior elements. For example, for the element with two-layer DOI, $n = 4$ for the interior elements and $n = 3$ for the exterior elements.

The Kriging shape functions $N_a(x)$, $a = 1, 2. ..., n$ are obtained by solving the Kriging system of equations [2,4,8], that is,

$$\mathbf{R}\boldsymbol{\lambda} + \mathbf{P}\boldsymbol{\mu} = \mathbf{r}(x) \tag{7a}$$

$$\mathbf{P}^{\mathrm{T}}\boldsymbol{\lambda} = \mathbf{p}(x) \tag{7b}$$

where

$$\mathbf{R} = \begin{bmatrix} C(h_{11}) & \dots & C(h_{1n}) \\ \dots & \dots & \dots \\ C(h_{n1}) & \dots & C(h_{nn}) \end{bmatrix}; \mathbf{P} = \begin{bmatrix} p_1(x_1) & \dots & p_m(x_1) \\ \dots & \dots & \dots \\ p_1(x_n) & \dots & p_m(x_n) \end{bmatrix} \tag{7c}$$

$$\boldsymbol{\lambda} = [\lambda_1 \quad \dots \quad \lambda_n]^{\mathrm{T}}; \boldsymbol{\mu} = [\mu_1 \quad \cdots \quad \mu_m]^{\mathrm{T}} \tag{7d}$$

$$\mathbf{r}(x) = [C(h_{1x}) \quad C(h_{2x}) \quad \dots \quad C(h_{nx})]^{\mathrm{T}} \tag{7e}$$

$$\mathbf{p}(x) = [p_1(x) \quad p_2(x) \quad \dots \quad p_m(x)]^{\mathrm{T}} \tag{7f}$$

In this equation, $\mathbf{R}$ is a $n \times n$ matrix of covariance between two random variables at nodes $x_1, ..., x_n$, in which $h_{ab} = x_b - x_a$, $a, b = 1,... n$; $\mathbf{P}$ is a $n \times m$ matrix of monomial values at the nodes where m is the number of monomial terms. Vector $\boldsymbol{\lambda}$ is an unknown $n \times 1$ vector of Kriging weights, which is identical to Kriging shape functions. Vector $\boldsymbol{\mu}$ is an unknown $m \times 1$ vector of Lagrange multipliers. On the right-hand side of eqns. (7a) and (7b), vector $\mathbf{r}(x)$ is a $n \times 1$ vector of covariance between random variables at the nodes and the point of interest, x, in which $h_{ax} = x - x_a$, $a = 1,..., n$; $\mathbf{p}(x)$ is a $m \times 1$ vector of monomial values at x. A necessary condition to make the Kriging equation system solvable (non-singular) is that $n \geq m$.

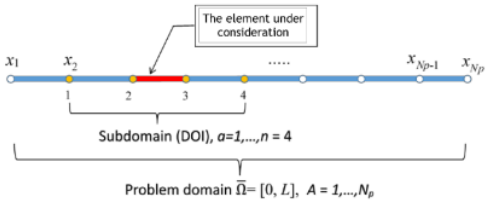

Figure 2. Beam Problem Domain, a Beam Element under Consideration and its Domain of Influencing Nodes

To construct Kriging shape functions using eqns. (7a) and (7b), one has to choose a correlation model and a set of polynomial bases. The correlation model is used to generate the covariance matrices $\mathbf{R}$ and $\mathbf{r}$, whereas the polynomial bases are used to generate matrices $\mathbf{P}$ and $\mathbf{p}$. Following previous works [7-8], the polynomial bases used in the present study are linear, quadratic, or cubic polynomial bases. Moreover, the Gaussian or quartic spline correlation models is utilized, that is,

$$\rho(h) = \exp\left(-\left(\theta_r \frac{h}{d}\right)^2\right) \tag{8a}$$

$$\rho(h) = \begin{cases} 1 - 6\left(\theta_r \frac{h}{d}\right)^2 + 8\left(\theta_r \frac{h}{d}\right)^3 - 3\left(\theta_r \frac{h}{d}\right)^4 & \text{for } 0 \leq \theta_r \frac{h}{d} \leq 1 \\ 0 & \text{for } \theta_r \frac{h}{d} > 1 \end{cases} \tag{8b}$$

Here, θ_r is a correlation parameter, h the distance between two points in the DOI, and d is the largest distance between two nodes in the DOI.

Substituting the approximate functions, eqns. (5) and (6), into the global weak form, eqn. (1), and carrying out the standard of finite element formulation gives the discretized matrix equation, that is,

$$\mathbf{K}\mathbf{D} = \mathbf{F}_{\mathrm{a}} + \mathbf{F}_q \tag{9}$$

In this equation, $\mathbf{K}$ is the structural stiffness matrix, that is,

$$\mathbf{K} = \sum_1^{N_e} \mathbf{k}_{\mathrm{b}}^e + \sum_1^{N_e} \mathbf{k}_{\mathrm{s}}^e \tag{10a}$$

$$\mathbf{k}_{\mathrm{b}}^e = \int_0^{L^e} \mathbf{B}_\theta^{e\,\mathrm{T}} EI \mathbf{B}_\theta^e \, dx; \mathbf{k}_{\mathrm{s}}^e = \int_0^{L^e} \mathbf{B}_\gamma^{e\,\mathrm{T}} GA_s \mathbf{B}_\gamma^e \, dx \tag{10b, c}$$

$\mathbf{D}$ is the structural nodal displacement vector, that is,

$$\mathbf{D} = [w_1 \quad \theta_1 \quad w_2 \quad \theta_2 \quad \cdots \quad w_{N_p} \quad \theta_{N_p}]^{\mathrm{T}} \tag{11}$$

$\mathbf{F}_{\mathrm{a}}$ is the vector of nodal applied forces, which for example shown in Fig. 1 is

$$\mathbf{F}_{\mathrm{a}} = \{P_0 \quad M_0 \quad 0 \quad 0 \quad \cdots \quad 0 \quad 0\}^{\mathrm{T}} \tag{12}$$

$\mathbf{F}_q$ is the equivalent nodal force vector due to a distributed load q, that is,

$$\mathbf{F}_q = \sum_1^{N_e} \mathbf{f}_q^e; \quad \mathbf{f}_q^e = \int_0^{L^e} \mathbf{N}_w{}^T q \, dx \tag{13a, b}$$

The order of matrix $\mathbf{K}$ is $2N_p \times 2N_p$ and the order of vectors $\mathbf{D}$, $\mathbf{F}_{\mathrm{a}}$ dan $\mathbf{F}_q$ are $2N_p$ 1. Matrices $\mathbf{k}_{\mathrm{b}}^e$ and $\mathbf{k}_{\mathrm{s}}^e$ are $2n \times 2n$ element stiffness matrices corresponding to bending and shear deformations, respectively, of

element number e, $e = 1, 2, ..., N_e$. Vector $\mathbf{f}_q^e$ is a $2n \times 1$ element equivalent nodal force vector due to q of element number e. Matrices $\mathbf{B}_\theta$ and $\mathbf{B}_\gamma$ in eqns. (10b) and (10c) are given as

$$\mathbf{B}_\theta^e = \frac{d}{dx}\mathbf{N}_\theta \tag{14a}$$

$$\mathbf{B}_\gamma^e = \frac{d}{dx}\mathbf{N}_w - \mathbf{N}_\theta \tag{14b}$$

The summation symbols in eqns. (10a) and (13a) denote the finite element assembly process, not the usual summation. The assembly process here involves all nodes in the DOI, not just elements nodes as in the standard FEM.

Discrete Shear Gap Technique

The use of the Kriging-based Timoshenko beam (K-beam) element model, eqn. (9), with exact integration of all integrals, gives much smaller displacement results than the true solutions for a very thin beam [7-8]. This phenomenon is well-known in the FEM and it is referred to as shear locking [15]. An approach to overcome the shear locking is the DSG technique [10, 16]. The basic idea of this technique is to replace the assumed displacement-based transverse shear strain over an element, $\gamma^e = w,^e_x - \theta^e$, with a substitute shear strain, $\overline{\gamma}^e$. This substitute strain field is obtained from the derivative of a substitute shear gap field [8,11]. In the previous work of Wong et al. [8], the DSG technique was applied in the K-beam models to eliminate the shear locking. However, the K-beam with the DSG was only effective for the K-beam-DSG elements with a cubic basis function and three-element-layer DOI. This section presents a modified implementation of the DSG technique to improve the performance of the previous K-beam-DSG element [8].

A shear gap field is defined as the increment of the deflection from a reference point x_0, due to shear strain, that is,

$$\Delta w_\gamma(x) = \int_{x_0}^{x} \gamma \, dx = w|_{x_0}^{x} - \int_{x_0}^{x} \theta \, dx \tag{15}$$

A discrete shear gap is the shear gap at a nodal point x_i, that is,

$$\Delta w_{\gamma i} = \Delta w_\gamma(x_i) = \int_{x_0}^{x_i} \gamma dx = w|_{x_0}^{x_i} - \int_{x_0}^{x_i} \theta \, dx \tag{16}$$

To eliminate shear locking, a *substitute* shear gap field is constructed by interpolating DSGs at several nodal points, viz.

$$\Delta\overline{w}_\gamma(x) = \sum_{i=1}^{n_{DSG}} I_i(x)\, \Delta w_{\gamma i} \tag{17}$$

where $I_i(x)$, $i = 1, 2, ..., n_{DSG}$ are nodal interpolation or shape functions for the substitute shear gap and n_{DSG} is the number of nodal shear gaps. A *substitute* shear strain field is then obtained by taking the derivative of the substitute shear gap field, that is,

$$\overline{\gamma}(x) = \sum_{i=1}^{n_{DSG}} I_{i,x}(x)\, \Delta w_{\gamma i} \tag{18}$$

In the previous work [8], the DSGs were evaluated at all nodal points in the DOI, thus $n_{DSG} = n$, and the interpolation functions used to construct the substitute shear gap were the Kriging shape functions used to interpolate the displacement fields, that is, $I_i(x) = N_i(x)$. In this study, the DSGs are only evaluated at the element nodal points and the interpolation functions used are the standard linear interpolants. Accordingly, the substitute shear gap field is given as

$$\overline{\gamma}(x) = \sum_{i=1}^{2} L_{i,x}(x)\, \Delta w_{\gamma i} \tag{19a}$$

where $L_{1,x}$ and $L_{2,x}$ are the derivatives of the standard linear shape functions, that is,

$$L_{1,x} = -\frac{1}{L^e}; \quad L_{2,x} = \frac{1}{L^e} \tag{19b, c}$$

where L^e is the element length.

In order to implement the present concept in a computer code, the shear gaps at the element nodes are firstly evaluated by taking the first node in the DOI under consideration (see Fig. 2) as the reference point and substituting the approximated rotation, eqn. (6a), into eqn. (16), that is,

$$\Delta w_{\gamma i} = (w_i - w_1) - \left(\int_{x_1}^{x_i} \mathbf{N}_\theta(x)\, dx\right)\mathbf{d} \tag{20}$$

Hence, the DSGs at the element nodes can be expressed as

$$\mathbf{w}_\gamma = \overline{\mathbf{B}}_{\gamma 2}\mathbf{d} \tag{21a}$$

where

$$\mathbf{w}_\gamma = \{\Delta w_{\gamma a} \quad \Delta w_{\gamma a+1}\}^T \tag{21b}$$

a, a+1: element node numbers

$$\overline{\mathbf{B}}_{\gamma 2} = \begin{bmatrix} -1 & -\int_{x_1}^{x_a} N_1 dx & 0 & -\int_{x_1}^{x_a} N_2 dx & \cdots & 1 & -\int_{x_1}^{x_a} N_a dx & \cdots & 0 & -\int_{x_1}^{x_a} N_n dx \\ -1 & -\int_{x_1}^{x_{a+1}} N_1 dx & 0 & -\int_{x_1}^{x_{a+1}} N_2 dx & \cdots & 1 & -\int_{x_1}^{x_{a+1}} N_{a+1} dx & \cdots & 0 & -\int_{x_1}^{x_{a+1}} N_n dx \end{bmatrix} \tag{21c}$$

$$\mathbf{d} = [w_1 \quad \theta_1 \quad w_2 \quad \theta_2 \quad \cdots \quad w_n \quad \theta_n]^T \tag{21d}$$

Writing eqn. (19a) in matrix forms,

$$\overline{\gamma}(x) = \overline{\mathbf{B}}_{\gamma 1}\mathbf{w}_\gamma \tag{22a}$$

$$\overline{\mathbf{B}}_{\gamma 1} = \frac{1}{L^e}[-1 \quad 1] \tag{22b}$$

Substituting eqn. (21a) into eqn. (22a) gives

$$\overline{\gamma}(x) = \overline{\mathbf{B}}_{\gamma 1}\,\overline{\mathbf{B}}_{\gamma 2}\mathbf{d} = \overline{\mathbf{B}}_\gamma \mathbf{d} \tag{23}$$

The implementation of the DSG concept is thus accomplished by replacing the matrix $\mathbf{B}_\gamma^e$ in the shear stiffness matrix, eqn. (10c), with the *substitute shear strain-displacement* matrix, $\overline{\mathbf{B}}_\gamma$.

Numerical Results

A series of numerical tests were carried out to investigate the performance of the Kriging-based beam element with the improved implementation of the DSG, which is referred to as K-beam-DSG1. The tests included shear locking, accuracy, and convergence tests. The test problems used were the same as in the

previous work [8]. The K-beam-DSG1 options used included linear, quadratic, and cubic polynomial bases with one to three element-layer DOIs and the Gaussian (G) and the quartic spline (QS) correlation functions. The correlation parameters were taken to be the middle values between the lower and upper bounds presented in the previous work [8]. However, since in all cases the results using the G and QS functions were nearly the same, only the results using the QS function were presented in this paper. Abbreviations of the form P*-*-QS were used to denote different K-beam-DSG1 options. The first asterisk represents the degree of a polynomial basis, whereas the second one indicates the number of DOI element layers. For example, P2-3-QS means K-beam element using a complete quadratic basis with three-element layer DOI and the quartic spline correlation function.

In all tests, the shear correction factor used is given as [17]

$$k = \frac{10(1+\nu)}{12+11\nu} \tag{24}$$

The integrals in the element stiffness matrices, eqns. (10b, c), the equivalent nodal force vectors, eqn. (13b), and the DSGs, eqn. (21c), were numerically evaluated using three Gaussian sampling points. The results were compared to those obtained using the K-beam of the previous work [8], which is referred to as K-beam-DSG0.

Shear Locking Tests

The test was carried out using a fixed-fixed supported beam subjected to a uniformly distributed load of q = 1 kN/m (Fig. 3). The material and geometrical parameters are E = 2000 kN/m^2, L = 10 m, b = 2 m, υ 0.3. To investigate the shear locking, the beam length-to-thickness ratio was varied from L/h = 5 (a relatively thick beam) to L/h = 10000 (an extremely thin beam). The beam was discretized using eight K-beam-DSG1 elements. The analysis results for the beam deflection at the midspan were recorded and normalized with the exact solution, that is,

$$w_{\text{exact}} = \frac{qL^4}{384EI} + \frac{qL^2}{8GA_s} \tag{25}$$

Table 1 presents the normalized beam deflection at the midspan for different length-to-thickness ratios, L/h, and different Kriging interpolation options. The table demonstrates that the present K-beam elements of all types are free from shear locking. In contrast, the K-beam-DSG0 elements are locking free only for the types of P1-1-QS and P3-3-QS. When the beam is relatively thick (L/h = 5 and 10), however, the present K-beam elements give a bit less accurate results compared to the previous elements.

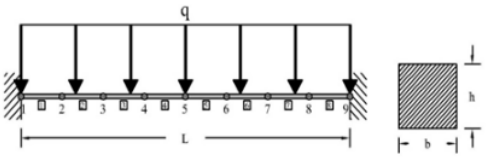

Figure 3. Fixed-fixed Supported Beam Modeled using Eight Beam Elements

Table 1. Normalized Midspan Deflections of the Fixed-fixed Beam with Different Length-to-thickness Ratios Modeled using Eight K-beam Elements

L/h	P1-1-QS		P1-2-QS	
	DSG1	DSG0 [8]	DSG1	DSG0 [8]
5	0.958	0.958	1.005	0.999
10	0.944	0.944	1.002	1.000
100	0.938	0.938	1.001	0.959
1000	0.938	0.938	1.001	0.206
10000	0.938	0.938	1.001	0.003

L/h	P2-2-QS		P2-3-QS		P3-3-QS	
	DSG1	DSG0 [8]	DSG1	DSG0 [8]	DSG1	DSG0 [8]
5	1.005	1.001	1.005	1.003	1.004	1.001
10	1.003	1.001	1.004	1.003	1.002	1.001
100	1.002	0.993	1.003	0.994	1.001	1.001
1000	1.002	0.540	1.003	0.505	1.001	1.001
10000	1.002	0.011	1.003	0.010	1.001	1.001

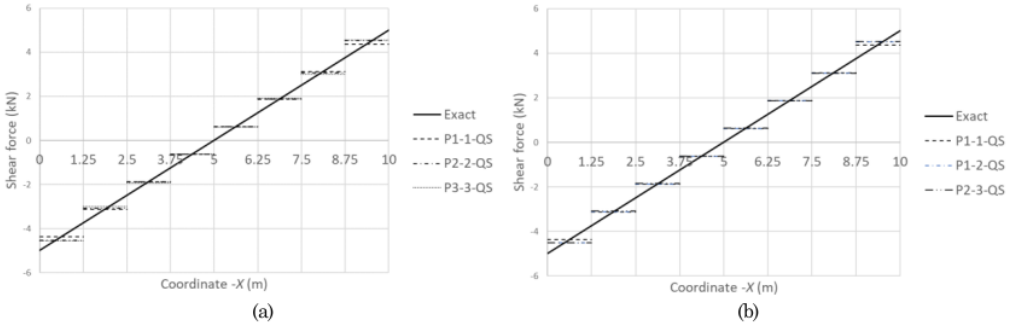

Figure 4. Shear Force Diagram for the Fixed-fixed Supported Beam with L/h = 10000 Obtained using the K-beam-DSG1 Elements of Different Types: (a) P1-1-QS, P2-2-QS, P3-3-QS; (b) P1-1-QS, P1-2-QS, P2-3-QS

The shear force diagrams for the beam of L/h =10000 resulting from the use of the K-beam-DGS1 of different types were plotted in Fig. 4 and compared to the exact shear force diagram. The figure shows that all of the K-beam-DSG1 elements give constant shear force distributions for each element (that is, piecewise constant). The shear force values resulting from different types of the K-beam-DSG1 are nearly the same for each element. The most accurate shear force prediction is approximately located at the middle point of each element. In contrast, the shear force distributions obtained using the K-beam-DSG0 elements [8] were fluctuating around the exact shear force line and were in great error for those obtained using the options of P1-2-QS and P2-3-QS. Thus, the present K-beam elements improved the shear force distribution results significantly.

Pure Bending Tests

Consider a cantilever beam subjected to an external bending moment, M, at the free end as shown in Fig. 5. The beam is under a pure bending condition with a constant moment M and zero shear force along the beam. The material and geometrical parameters were taken to be equal to those of the beam in the shear locking test and M = 1 kN-m. Two different length-to-thickness ratios were considered in this test, namely, L/h = 5 and L/h = 10000. The beam was discretized using four K-beam elements of different lengths as shown in the figure.

The analysis results of the deflection and rotation at the free end were observed and normalized to the analytical solutions, that is,

$$w_{\text{exact}} = \frac{ML^2}{2EI};\quad \theta_{\text{exact}} = \frac{ML}{EI} \tag{26}$$

In addition, the bending moments and shear forces at the fixed end were observed. The bending moments were then normalized to the analytical solution, M = 1. The shear forces, however, were not normalized since the exact shear force is zero.

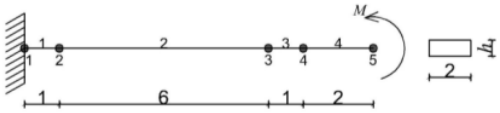

Figure 5. Cantilever Beam Modeled using Four Elements of Unequal Length

Table 2. Analysis Results for the Cantilever Beam of L/h = 10000 under Pure Bending, Modeled using Four K-beam-DSG1 Elements of Unequal Length with Different Element Types

K-beam-DSG options	$w_L/w_{L\text{exact}}$	$\theta_L/\theta_{L\text{exact}}$	$M_0/M_{0\text{exact}}$	V_0
P1-1-QS	1.0000000	1.0000000	1.0000000	6.52E-09
P1-2-QS	1.0000001	1.0000001	1.0000001	1.67E-08
P2-2-QS	1.0000001	1.0000001	1.0000002	2.07E-08
P2-3-QS	1.0000002	1.0000001	1.0000003	1.23E-08
P3-3-QS	1.0000001	1.0000000	1.0000001	9.55E-09

For the case of the beam of L/h = 5, all of the resulting deflections, rotations, and shear forces obtained using different K-beam-DGS1 are exact within computer double precision accuracy. The bending moments are very close to the exact value, that is,14 digits accurate. The results for the beam of L/h = 10000 were presented in Table 2. It is seen that the deflections, rotations, and bending moments have at least seven-digit accuracy. The errors for the shear forces are on the order of 10^{-8} or 10^{-9}. In comparison to the previous K-beam-DSG elements [8], the performance of the improved K-beam-DSG in this problem is similar.

It is worth mentioning here that this constant bending test may be regarded as a type of patch test for beam finite elements [11]. A beam element passes the test if it can reproduce exact results (within computer accuracy). Therefore, the K-beam-DGS1 elements pass the pure bending patch test since they produced the exact or nearly exact results.

Assessment of Accuracy and Convergence

A cantilever beam subjected to a triangular-distributed load (Figure 6) was utilized to assess the performance of the present K-beam elements in terms of accuracy and convergence. The geometric, material, and load data were taken as follows: L = 4 m, L/h = 8, b = 2 m, E = 1000 kN/m^2, υ = 0.3, and $q_0 = q(0)$ = 1 kN/m. The beam was modeled using different numbers of K-beam elements, that is, 4, 8, 16, and 32 elements. The results of the tip deflections, the bending moments at the fixed end, and the shear forces at the fixed end were observed and normalized to their corresponding analytical solutions [18], that is,

$$w_L = \frac{q_0 L^4}{30EI}\left(1+\frac{5}{12}\phi\right);\quad \phi = \frac{12+11\nu}{5}\left(\frac{h}{L}\right)^2 \tag{27a, b}$$

$$M_0 = \tfrac{1}{6}q_0L^2\ ,\ Q_0 = \tfrac{1}{2}q_0L \tag{28a, b}$$

Table 3 presented all of the normalized analysis results using different types of K-beam-DSG1 elements. The table shows that the elements give highly accurate results of the deflections and bending moments and reasonably accurate results of the shear forces. Moreover, the table demonstrates the excellent convergence characteristics of the K-beam-DGS1 elements.

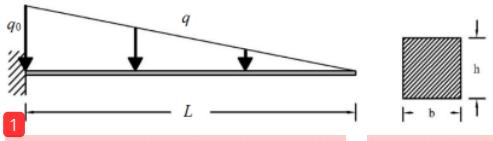

Figure 6. Cantilever Beam Subjected to a Linearly Distributed Force q

Table 3. Analysis Results for the Cantilever Beam ($L/h = 8$) Subjected to a Linearly Distributed Force, Modeled using Different Numbers, *Nelem*, and Different Types of K-beam-DSG1 Elements

(a) Normalized tip deflection

Nelem	P1-1-QS	P1-2-QS	P2-2-QS	P2-3-QS	P3-3-QS
4	1.02489	1.00324	1.00359	1.00311	1.00000
8	1.00634	0.99888	1.00026	1.00017	1.00000
16	1.00159	0.99946	1.00002	1.00001	1.00000
32	1.00040	0.99983	1.00000	1.00000	1.00000

(b) Normalized fixed-end bending moment

Nelem	P1-1-QS	P1-2-QS	P2-2-QS	P2-3-QS	P3-3-QS
4	0.71094	0.80281	0.93369	0.90683	1.00305
8	0.83496	0.89753	0.98121	0.97279	1.00272
16	0.91199	0.94800	0.99503	0.99270	1.00094
32	0.95457	0.97383	0.99872	0.99811	1.00027

(c) Normalized fixed-end shear force

Nelem	P1-1-QS	P1-2-QS	P2-2-QS	P2-3-QS	P3-3-QS
4	0.77083	0.81296	0.82066	0.81910	0.83628
8	0.88021	0.90459	0.90829	0.90723	0.91496
16	0.93880	0.95182	0.95363	0.95295	0.95684
32	0.96908	0.97579	0.97669	0.97631	0.97826

The higher degree of the polynomial basis used, as expected, the more accurate the results obtained for the same number of elements. The use of the K-beam-DSG1 with cubic basis, P3-3-QS, can reproduce the exact tip deflection even though using four elements.

To compare the results to those obtained using the K-beam-DSG0, consider the cases studied in Wong et al. [8], that is, the cantilever beam of the length-to-thickness rations $L/h = 8$ (moderately thick beam), $L/h = 1$ (extremely thick beam), and $L/h = 10000$ (extremely thin beam). The beam was analyzed using the K-beam-DSG1 element of P3-3-QS only because this element was the only type of the K-beam-DSG0 element that was used in Wong et al. [8]. Comparison of the results of the tip deflections, bending moments at the fixed end, and shear forces at the fixed end were presented in Table 4. It is seen that for the cases of the thick beams, the accuracy of the deflections and bending moments from the K-beam-DSG1 and DSG0 P3-3-QS is approximately equal. However, the shear forces obtained using the present element are less accurate, in particular, for the course mesh discretization (*Nelem* = 4). For the case of the extremely thin beam, the deflections obtained using both methods remain very accurate, but the accuracy of the bending moments and shear forces obtained using the K-beam-DSG0 element declines. It is apparent that the performance of the K-beam-DSG1 elements is not affected by the change of the beam thickness. In contrast, the performance of the K-beam-DSG0 elements decreases as the beam becomes thinner.

Table 4. Normalized Analysis Results for the Cantilever Beam of Different Length-to-thickness Ratios Subjected to a Linearly Distributed Force, Modeled using Different Numbers, *Nelem*, of the K-beam-DSG1 and K-beam-DSG0 P3-3-QS [8] Elements

(a) Moderately thick beam, $L/h = 8$

Nelem	Deflection		Bending Moment		Shear Force	
	DSG1	DSG0	DSG1	DSG0	DSG1	DSG0
4	1.00000	0.99989	1.00305	0.99972	0.83628	1.03397
8	1.00000	0.99999	1.00272	1.00190	0.91496	1.00210
16	1.00000	1.00000	1.00094	1.00074	0.95684	1.00022
32	1.00000	1.00000	1.00027	1.00022	0.97826	1.00003

(b) Extremely thick beam, $L/h = 1$

Nelem	Deflection		Bending Moment		Shear Force	
	DSG1	DSG0	DSG1	DSG0	DSG1	DSG0
4	1.00000	0.99995	1.00305	1.00055	0.83628	1.00097
8	1.00000	1.00000	1.00272	1.00192	0.91496	1.00019
16	1.00000	1.00000	1.00094	1.00074	0.95684	1.00004
32	1.00000	1.00000	1.00027	1.00022	0.97826	1.00001

(c) Extremely thin beam, $L/h = 10000$

Nelem	Deflection		Bending Moment		Shear Force	
	DSG1	DSG0	DSG1	DSG0	DSG1	DSG0
4	1.00000	0.99989	1.00305	0.95561	0.83628	2.79078
8	1.00000	0.99999	1.00272	0.95087	0.91496	2.58935
16	1.00000	1.00000	1.00094	0.98499	0.95684	0.61493
32	1.00000	1.00000	1.00027	0.99917	0.97826	0.97775

Figure 7 shows the shear force diagram for the beam of L/h =8, obtained using four present and previous P3-3-QS K-beam elements, compared to the true shear force diagram. It is seen that the previous beam element gives a more accurate shear force distribution compared to the present element. This confirms that for the case of thick beams, the present beam element is less accurate in predicting the shear force field. However, if the beam becomes thinner, the accuracy of the present element remains the same while the accuracy of the previous element decreases.

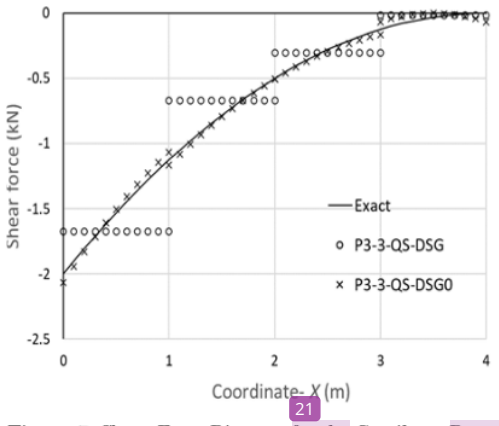

Figure 7. Shear Force Diagram for the Cantilever Beam with $L/h = 8$ Obtained using the K-beam-DSG1 and K-beam-DSG0 Elements of P3-3-QS

Conclusions

In the previous work [8], the DSG technique was applied to eliminate shear locking in Kriging-based Timoshenko beam elements (referred to as K-beam-DSG0 elements in this paper). However, it was only effective for the K-beam using a cubic basis and three-element layer DOI. In this work, the implementation of the DSG technique has been modified in an attempt to improve the K-beam-DSG0 elements. The modification made was to change the formulation of the substitute DSG interpolation from a Kriging interpolation of nodal shear gaps at all nodes in the DOI to a linear interpolation of nodal shear gaps at the element nodes only. The numerical tests showed that the modified K-beam-DSG elements (referred to K-beam-DSG1 elements) of all types are truly free from shear locking, pass the pure bending test, can give highly accurate results of the deflection and bending moment with a relatively small number of elements, and have excellent convergence characteristics. The accuracy of the K-beam-DSG1 elements is not affected by a change in beam thickness. The resulting shear force distributions, however, do not match the true shear force distribution and are piecewise constant.

The present K-beam-DSG1 formulation gives insight regarding the implementation of the DSG technique in the framework of Kriging-based FEM. Further research may be directed to the extension of the present elements for vibration analysis, buckling analysis, and geometrically nonlinear analysis. Another research direction that may be taken is an implementation of the DSG technique in Kriging-based curved beam elements, plate bending elements, and shell elements.

References

1. Plengkhom, K. and Kanok-Nukulchai, W., An Enhancement of Finite Element Method with Moving Kriging Shape Functions, *International Journal of Computational Methods*, 02(04), 2005, pp. 451–475.
2. Wong, F.T. and Kanok-Nukulchai, W., Kriging-based Finite Element Method : Element-By-Element Kriging Interpolation, *Civil Engineering Dimension*, 11(1), 2009, pp. 15–22.
3. Kanok-Nukulchai, W, Wong, F.T., and Sommanawat, W., Generalization of FEM using Node-Based Shape Functions, *Civil Engineering Dimension*, 17(3), 2015, pp. 152–157.
4. Wong, F.T. and Kanok-Nukulchai, W., On the Convergence of the Kriging-based Finite Element Method, *International Journal of Computational Methods*, 06(01), 2009, pp. 93–118.
5. Wong, F.T. and Kanok-Nukulchai, W., On Alleviation of Shear Locking in the Kriging-Based Finite Element Method, *Proceedings of International Civil Engineering Conference "Towards Sustainable Engineering Practice"*, Surabaya, Indonesia, August 25-26, 2006, pp. 39–47.
6. Wong, F. T., Kriging-based Finite Element Method for Analyses of Plates and Shells, *Doctoral Dissertation*, Asian Institute of Technology, Pathumthani, 2009.
7. Wong, F.T. and Syamsoeyadi, H., Kriging-based Timoshenko Beam Element for Static and Free Vibration Analyses, *Civil Engineering Dimension*, 13(1), 2011, pp. 42–49.
8. Wong, F.T., Sulistio, A., and Syamsoeyadi, H., Kriging-Based Timoshenko Beam Elements with the Discrete Shear Gap Technique, *International Journal of Computational Methods*, 15(7), 2018, pp. 1850064-1–27.
9. Koschnick, F., Bischoff, M., Camprubí, N., and Bletzinger, K.U., The Discrete Strain Gap Method and Membrane Locking, *Computer Methods in Applied Mechanics and Engineering*, 194(21-24), 2005, pp. 2444–2463.
10. Bletzinger, K.U., Bischoff, M., and Ramm, E., A Unified Approach for Shear-Locking-Free Triangular and Rectangular Shell Finite Elements, *Computers and Structures*, 75(3), 2000, pp. 321–334.
11. Wong, F.T. and Sugianto, S., Study of the Discrete Shear Gap Technique in Timoshenko Beam Elements, *Civil Engineering Dimension*, 19(1), 2017, pp. 54–62, 2017.
12. Wong, F.T, Gunawan, J., Agusta, K., Herryanto, and Tanaya, L.S., On the Derivation of Exact Solutions of a Tapered Cantilever Timoshenko Beam, *Civil Engineering Dimension*, 21(2), 2019, pp. 89–96.
13. Hughes, T.J.R., *The Finite Element Method: Linear Static and Dynamic Finite Element Analysis*, Prentice-Hall, New Jersey, 1987.
14. Garikipati, K., Introduction to Finite Element Methods, *Open Michigan*, 2013. https://open.umich.edu/find/open-educational-resources/engineering/introduction-finite-element-methods (accessed Jan. 23, 2019).
15. Onate, E., *Structural Analysis with the Finite Element Method-Vol. 2: Beams, Plates and Shells*, First edition, Springer, Barcelona, 2013.
16. Bischoff, M., Koschnick, F., and Bletzinger, K.Y, Stabilized DSG Elements – A New Paradigm in Finite Element Technology, *Proceedings of the 4th European LS-DYNA Users Conference*, Ulm, Germany, May 22-23, 2003.
17. Cowper, G.R., The Shear Coefficient in Timoshenko's Beam Theory, *Journal of Applied Mechanics*, 33(2), 1966, pp. 335–340.
18. Friedman, Z. and Kosmatka, J.B., An Improved Two-node Timoshenko Beam Finite Element, *Computers and Structuers*, 47(3), 1993, pp. 473–481.

My latest paper to CED

ORIGINALITY REPORT

22%	20%	9%	1%
SIMILARITY INDEX	INTERNET SOURCES	PUBLICATIONS	STUDENT PAPERS

PRIMARY SOURCES

1	repository.petra.ac.id Internet Source	10%
2	www.journaltocs.ac.uk Internet Source	4%
3	moam.info Internet Source	2%
4	Eugenio Oñate. "Structural Analysis with the Finite Element Method Linear Statics", Springer Science and Business Media LLC, 2013 Publication	1%
5	123dok.com Internet Source	1%
6	www.thefreelibrary.com Internet Source	<1%
7	campus2.iust.ac.ir Internet Source	<1%
8	bayanbox.ir Internet Source	<1%

9	shellbuckling.com Internet Source	<1%
10	M. Bischoff. "Models and Finite Elements for Thin-Walled Structures", Encyclopedia of Computational Mechanics, 11/15/2004 Publication	<1%
11	T. NGUYEN-THOI, G. R. LIU, H. NGUYEN-XUAN. "ADDITIONAL PROPERTIES OF THE NODE-BASED SMOOTHED FINITE ELEMENT METHOD (NS-FEM) FOR SOLID MECHANICS PROBLEMS", International Journal of Computational Methods, 2011 Publication	<1%
12	Submitted to University of Nottingham Student Paper	<1%
13	CHUN-LONG ZHENG, HAI-PING ZHU, LIN-SEN XIE, JIAN-PING FANG. "SINGLE AND MULTIPLE VALUED LOCALIZED EXCITATIONS OF BOITI-LEON-PEMPINELLI SYSTEM IN (2+1)-DIMENSIONS VIA A MAPPING METHOD", International Journal of Modern Physics B, 2012 Publication	<1%
14	calhoun.nps.edu Internet Source	<1%
15	Eugenio Oñate. "Extended rotation-free plate and beam elements with shear deformation	<1%

effects", International Journal for Numerical Methods in Engineering, 2010
Publication

16	Guoyong Jin, Chuanmeng Yang, Zhigang Liu. "Vibration and damping analysis of sandwich viscoelastic-core beam using Reddy's higher-order theory", Composite Structures, 2016 Publication	<1 %
17	www.dcs.gla.ac.uk Internet Source	<1 %
18	Engineering Computations, Volume 17, Issue 3 (2006-09-19) Publication	<1 %
19	M.A.R. Loja, J.I. Barbosa, C.M. Mota Soares. "Analysis of sandwich beam structures using kriging based higher order models", Composite Structures, 2015 Publication	<1 %
20	Nishidate, Y, and G Nikishkov. "Continuum and Atomic-Scale Finite Element Modeling of Multilayer Self-Positioning Nanostructures", Computational Finite Element Methods in Nanotechnology, 2012. Publication	<1 %
21	Raju, I, and D Phillips. "Radial Basis Meshless Local Petrov-Galerkin Method for Thick Beams", 45th AIAA/ASME/ASCE/AHS/ASC	<1 %

	Structures Structural Dynamics & Materials Conference, 2004. Publication	
22	hdl.handle.net Internet Source	<1 %
23	imechanica.org Internet Source	<1 %
24	journals.sagepub.com Internet Source	<1 %
25	techscience.com Internet Source	<1 %
26	www.msc-les.org Internet Source	<1 %
27	Chassaing, Jean-Camille, Xesús Nogueira, and Sofiane Khelladi. "Moving Kriging reconstruction for high-order finite volume computation of compressible flows", Computer Methods in Applied Mechanics and Engineering, 2013. Publication	<1 %
28	"Recent Developments in the Theory of Shells", Springer Science and Business Media LLC, 2019 Publication	<1 %
29	Zhu, P.. "Free vibration analysis of moderately thick functionally graded plates by local	<1 %

Kriging meshless method", Composite Structures, 201110

Publication

Exclude quotes	On	Exclude matches	< 5 words
Exclude bibliography	On		